

Elastic metamaterial rod for mode filtering in ultrasonic applications

S.K. Sikundapuram Ramesh, M. Chitnaduku
Thippeswamy^{*}, P. Rajagopal and K. Balasubramaniam

The proposed 1D elastic metamaterial rod finds application in non-destructive evaluation, as a filter in the transduction side, where only the torsional and flexural modes need to be generated by isolating longitudinal modes. In this Letter, this is achieved by obtaining a wide bandgap in low-frequency ultrasound regime. The novelty of the proposed design arises from the use of a high impedance mismatch between the materials selected for the rod. The proposed concept is demonstrated and verified with numerical simulations. The effectiveness of the proposed technique is confirmed by comparing the results obtained from the rod made of a single material.

Introduction: Modulation and control of wave propagation in elastic materials have many applications and are of much interest in the non-destructive evaluation (NDE) community. In the last two decades, researchers have shown considerable interest in the field of acoustic/elastic metamaterials (AMM/EMM) for the manipulation of elastic waves. AMM/EMM are artificially structured composite materials that exhibit non-intuitive properties, which finds applications in negative refraction [1], focusing [2], wave manipulation [3], and frequency filters [4]. The current study is focused on developing EMM waveguide rods for filtering a specific frequency range by creating bandgaps in the ultrasonic regime. Some of the other applications apart from NDE, where a wider bandgap is crucial include waveguiding, trapping, and vibration isolation, among other possibilities.

In the last few years, research groups have proposed various structures of 1D EMM rods made of different materials to achieve bandgap in acoustic/sonic applications. A 1D EMM rod consisting of porous silicon carbide sandwiched between rubber layers demonstrated the bandgap in the acoustic frequency range [5]. A lightweight EMM rod, consisting of rubber and enclosed by the metal ring, was proposed to achieve bandgap at an audible frequency range. Bandgaps were controlled by tuning the arc angle of the rubber layer and by the number of arc-shaped rubbers [6]. In the literature, various structures consisting of rods/shafts [7] or plates [8] made of different materials have been proposed to achieve wider bandgaps in the acoustic frequency regime. Even though the plate structures [9, 10] have demonstrated the bandgaps in the ultrasonic region, very little attention has been drawn towards achieving the bandgaps using rods in low-frequency ultrasonic regime, which is addressed in this Letter by using two different materials.

The Letter is organised as follows: the first section presents the design of the 1D bimetallic elastic metamaterial. The enhanced bandgaps obtained by improvised design are presented later. Followed by this, the optimum number of baffles required to achieve the bandgap is studied. The application of the EMM rod in NDE is discussed, and finally, the paper concludes with future directions.

Design of a 1D bimetallic EMM: Bandgaps are mainly formed by two different approaches, namely, Bragg scattering and local resonance. Inclusions in the host material play an essential role in increasing the width of the bandgap. High impedance mismatch is one of the critical parameters in achieving bandgaps, which can be attained either by changing the dimensions of the inclusions in the host material or having different material properties from the host material. This Letter focuses on achieving the bandgaps by virtue of different material combinations. To sum up, we are proposing two different cases to achieve bandgap. The first case is concerned with only material impedance mismatch, and the second case includes both material and geometrical impedance mismatch. One of the critical parameters in designing this EMM rod is the selection of materials, with high impedance mismatch. Table 1 shows the list of commonly available materials used in this study.

Table 1: Acoustic impedance of various materials used in the current study

Material	Al	Brass	Steel	Mo
acoustic impedance	17	36	46	64

Case I: EMM rod with different material impedance: The proposed 1D bimetallic EMM rod consists of two different materials, A and B, of the same diameter. They are arranged parallel to each other, along the wave propagation direction. Material A is the host medium and material B is the embedded material. The alternate layer of materials A and B forms one unit cell. The designed EMM rod is circular in cross-section of radius $R=5$ mm and unit cell length, ' L '. Figs. 1a and b illustrate the geometry of the EMM rod and unit cell, respectively. Furthermore, in this Letter, aluminium (Al) is considered as the host material (material A), and the embedding material (material B) will be either brass or steel or molybdenum (Mo).

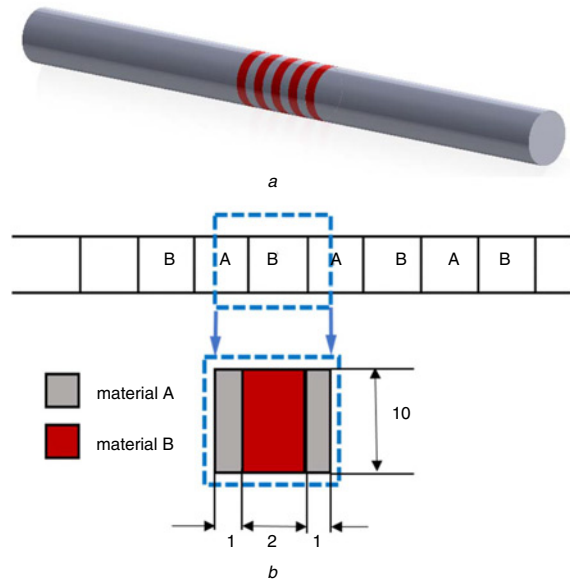


Fig. 1 Illustration of the proposed bimetallic rod

a Schematic of 1D bimetallic EMM rod

b Unit-cell consisting of alternate different material layers indicating the dimensions. All the dimensions are in mm

The Bragg condition to calculate the unit cell dimension for the selected excitation frequency is as given below

$$L = n \left(\frac{\lambda}{2} \right) \quad (1)$$

where L is the unit cell length of the periodic system, λ is the wavelength of the propagating wave in the rod, and $n = 1, 2, 3, \dots$

Dispersion diagram of the EMM rod: The frequency-wave number dispersion plot for the proposed design is obtained using the Eigen solver in the commercially available Finite Element (FE) package (see: Reference Manual version 5.2, COMSOL Multiphysics, COMSOL AB Stockholm, Sweden 2015, <https://www.comsol.com/support>). The unit cell was modelled as an axisymmetric FE model to obtain the dispersion curves. These curves are obtained by applying the periodic boundary conditions on a unit cell at the interfaces between the adjacent unit cells, which is defined by the Floquet–Bloch theorem. According to this theorem

$$\mathbf{u}(n) = e^{i(k \cdot n)} \mathbf{u}_k(n) \quad (2)$$

where $\mathbf{u}_k(n)$ is the vector of wave amplitude, n represents nodes at the boundary, \mathbf{k} is the wave vector. The Floquet–Bloch periodicity boundary condition was applied to the sides of the unit cell along the wave propagation direction (x -direction),

$$\mathbf{u}(x + L) = \mathbf{u}(x) e^{i(k_x L - \omega t)} \quad (3)$$

where k_x is the component of the Bloch wave vector in the x -direction, L is the lattice constant, and $\mathbf{u}(x)$ is the magnitude of lattice periodic displacement field.

Following the above method, the dispersion curves for different material combinations such as Al–brass, Al–steel, and Al–Mo were obtained and are as shown in Fig. 2. It is observed that the selection of material will influence the bandgaps, which occurs due to impedance mismatch. From Table 2, it is seen that the bandgap obtained from

Al–Mo is broader than that of the other two combinations. Hence, Al–Mo is selected as the materials for the EMM rod.

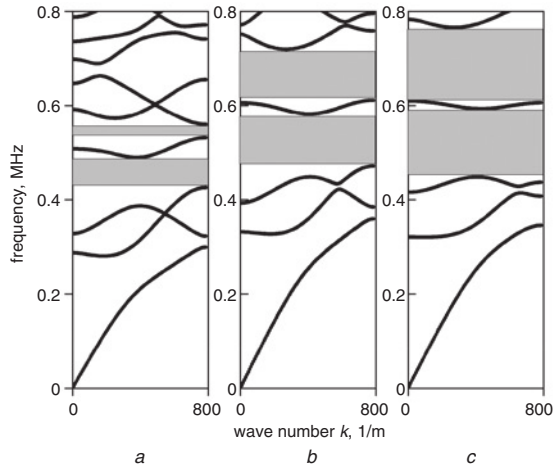


Fig. 2 Band diagrams obtained from different material combinations

- a Al–brass
- b Al–steel
- c Al–Mo

Table 2: Bandgap comparison between various material combinations

Bimetallic rod	First bandgap, kHz	Second bandgap, kHz
Al–brass	430–485	531–560
Al–steel	475–580	615–715
Al–Mo	450–590	610–760

To further improve the bandgap, we are introducing geometrical impedance mismatch along with the material impedance. The geometrical impedance mismatch is created by increasing the diameter of material B (Mo) than material A (Al). The additional material will act like a local resonator, which helps to achieve a wider bandgap.

Case II: EMM rod with geometry impedance along with material impedance: In this section, geometry impedance mismatch is introduced to the previous case by changing the diameter of material B (Mo) by 2 mm, which will act as a baffle. Fig. 3a illustrates the design of the EMM rod with baffles and Fig. 3b shows the unit cell indicating the dimensions, respectively.

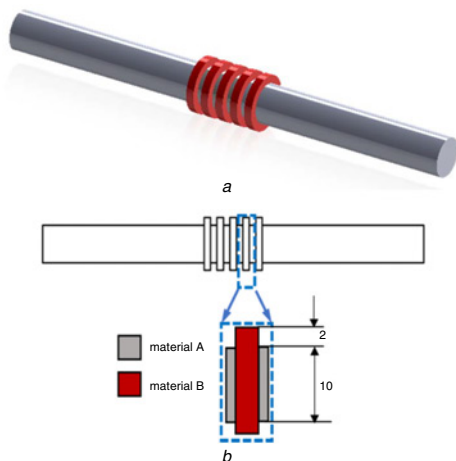


Fig. 3 Design of the elastic metamaterial rod with baffles

- a Schematic representation of EMM rod with baffles
- b Unit cell of proposed design (case II), along with dimensions. All dimensions are in mm

The bandgap formed after the introduction of baffles is as depicted in Fig. 4. As expected there is an increase in the bandgap width due to the change in the design of the unit-cell. The increase in diameter of

the second material (Mo) will act as a local resonator, and due to this width of the bandgap is increased. Table 3 gives a comparison of case (i) and case (ii) with Al–Mo material combination.

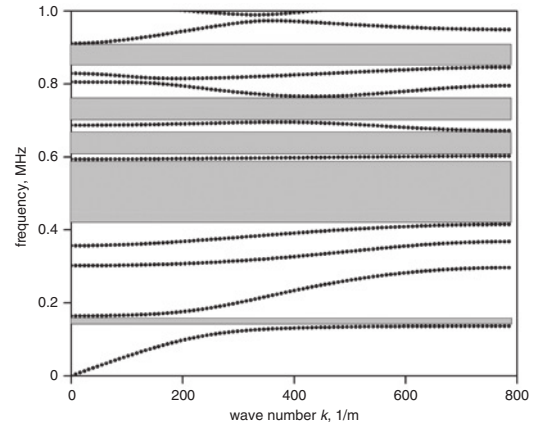


Fig. 4 Band structure observed from EMM rod with baffles

Table 3: Comparison of the width of bandgaps

Al–Mo EMM rod	First bandgap	Second bandgap	Third bandgap	Fourth bandgap	Fifth bandgap
case I	450–590	610–760	—	—	—
case II	140–160	420–590	610–665	700–760	850–900

Effect of the number of baffles on the bandgaps: The commercially available FE package (see: ABAQUS User Manual version 6.12, Dassault Systems, Providence, RI, USA, 2014, <https://www.3ds.com/products-services/simulia/products/abaqus/>) in dynamic/explicit module was used to understand the effect of the number of baffles on the bandgaps. The computational complexity of the model is reduced by considering an axisymmetric analysis. The FE model was meshed with a four-node bilinear axisymmetric quadrilateral (CAX4R) element. The input was a Hanning windowed tone burst signal, with a frequency centred at 500 kHz. The fast Fourier transform of the monitored a-scan for the different number of baffles is shown in Fig. 5. It is observed that as the number of baffles increases the range of bandgaps also increases, and beyond five baffles, there is no significant change in the bandgap. Hence, five baffles were chosen for further analysis.

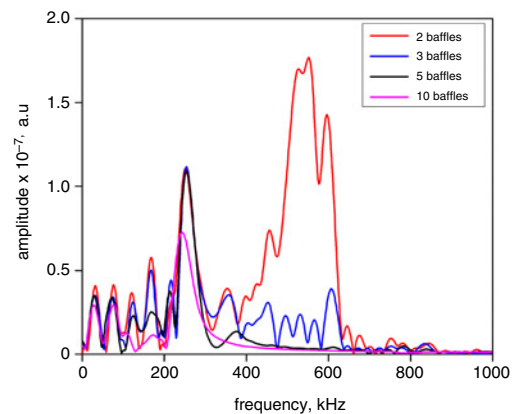


Fig. 5 Effect of number of baffles on bandgap

Transmission analysis: The performance of the proposed design is observed by considering a finite length of the structure. The length of the EMM rod with baffles is 120 mm, including five unit cells, where each unit cell length is 4 mm. Longitudinal waves at a frequency of 500 kHz are excited and received at the other end of the structure. The a-scans collected at the exciting side and receiving side were used to compute the transmission spectra at various frequencies. As shown in Fig. 6, the transmission spectra were obtained numerically, and are given by

$$\text{Transmission} = \frac{a_r^2}{a_i^2} \quad (4)$$

where a_t is the amplitude of the transmitted signal and a_i is the amplitude of the incident signal. It is observed that the frequency bandgap obtained from the transmission spectra (see Fig. 6) is matching with the bandgap predicted from the dispersion analysis, as shown in Fig. 4.

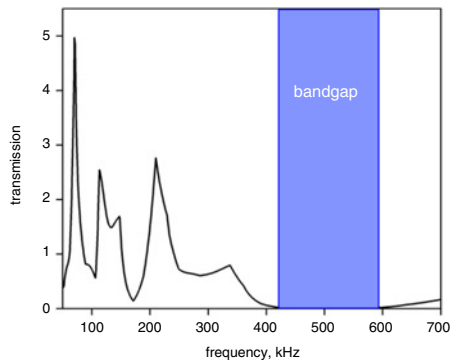


Fig. 6 Transmission spectra of EMM rod with baffles computed along direction of wave propagation

In NDE applications, selective mode of wave propagation is a challenging task. This issue can be addressed by making use of bandgaps, wherein specific propagation wave modes can be suppressed. To further understand the suppression of modes, modal analysis was carried out on the 3D unit cell (shown in Fig. 3b), and the corresponding dispersion curves are shown in Fig. 7a. We can observe two narrow complete bandgaps (shown in red in Fig. 7a), where no modes exist. By comparing these dispersion curves with that obtained from the axisymmetric unit cell (shown in Fig. 7b), we can observe the propagation of torsional and flexural modes in the bandgap of frequency range 410–570 kHz. This confirms that polarised bandgap exists from 410 to 570 kHz, where only the longitudinal wave modes cannot propagate. Thus, the proposed EMM rod can act as a stopband filter for longitudinal modes, and a pass band filter for torsional and flexural modes.

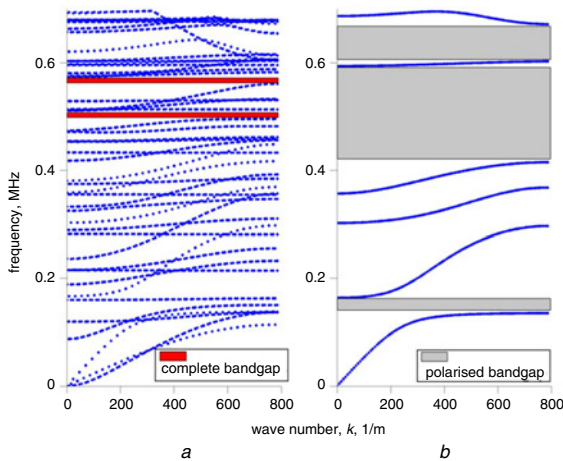


Fig. 7 Dispersion diagram illustrating
a Complete bandgap
b Polarised bandgap

Further to demonstrate the effectiveness of this design, a study was carried out by comparing the proposed design (case II) dispersion curves with EMM rod made of a single material (Al), by keeping all the geometric and simulation parameters constant. The comparison of dispersion curves is as depicted in Fig. 8. The blue-shaded area represents the width of the bandgap from a single material. The red-shaded area represents the bandgap achieved from the bimetallic EMM rod. It was observed that the bandgap obtained using the proposed design is wider than that of a single material. The wider bandgap obtained from the proposed EMM rod can further be used in other applications such as vibration isolation and wave guiding apart from NDE.

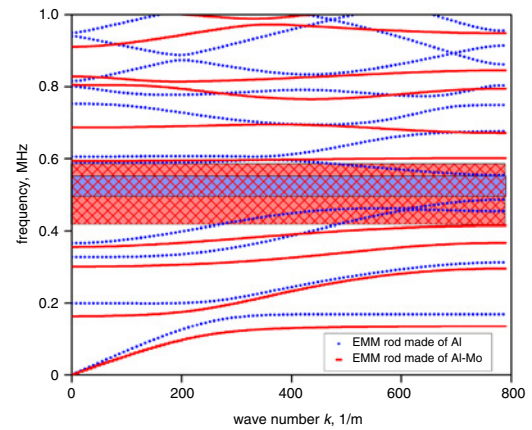


Fig. 8 Comparison of dispersion curves achieved by using single and bimetallic EMM rod

Conclusion: To conclude, we have achieved wide bandgaps by using the proposed bimetallic EMM rod in the ultrasonic regime. Various material combinations were studied to obtain a wider bandgap, with less number of baffles. A wide bandgap of 420–590 kHz is demonstrated by using the bimetallic EMM rod. This design approach for the EMM rod will be useful in NDE applications, where the longitudinal modes need to be mitigated. Furthermore, the bandgap can be improved by varying the geometrical parameters of the embedded material in the host medium.

© The Institution of Engineering and Technology 2020
Submitted: 25 May 2020 E-first: 30 June 2020
doi: 10.1049/el.2020.1576

One or more of the Figures in this Letter are available in colour online.

S.K. Sikundalapuram Ramesh, M. Chitnaduku Thippeswamy, P. Rajagopal and K. Balasubramaniam (Centre for Non-Destructive Evaluation, Indian Institute of Technology Madras, Chennai-600036, India)

✉ E-mail: manjunath.ct@gmail.com

References

- Zhang, X., and Liu, Z.: 'Negative refraction of acoustic waves in two-dimensional phononic crystals', *Appl. Phys. Lett.*, 2004, **85**, (2), pp. 341–343, doi.org/10.1063/1.1772854
- Manjunath, C.T., and Rajagopal, P.: 'Lensing in the ultrasonic domain using negative refraction induced by material contrast', *Sci. Rep.*, 2019, **9**, (6368), pp. 1–8, doi: 10.1038/s41598-019-42655-3
- Kuchibhatla, S.A.R., and Rajagopal, P.: 'A transformation elasticity based device for wavefront manipulation', *NDT E Int.*, 2019, **102**, pp. 304–310, doi: 10.1016/j.ndteint.2019.01.006
- Zhu, H., and Fabio, S.: 'Metamaterial based embedded acoustic filters for structural applications', *AIP Adv.*, 2013, **3**, (9), pp. 1–8, doi.org/10.1063/1.4822157
- Ahmed, M., and Ashour, M.A.: 'Locally resonant phononic crystals at low frequencies based on porous Sic multilayer', *Sci. Rep.*, 2019, **9**, pp. 1–12, doi.org/10.1038/s41598-019-51329-z
- Li, L., Lv, R., Cai, A., et al.: 'Low-frequency vibration suppression of a multi-layered elastic metamaterial shaft with discretized scatter', *J. Phys. D, Appl. Phys.*, 2019, **52**, (5), pp. 1–10, doi.org/10.1088/1361-6463/aaef66
- Munday, J.N., Brad Bennett, C., and Robertson, W.M.: 'Band gaps and defect modes in periodically structured waveguides', *J. Acoust. Soc. Am.*, 2002, **112**, (4), pp. 1353–1358, doi: 10.1121/1.1497625
- Coffy, E., Laverne, T., Addouche, M., et al.: 'Ultra-wide acoustic band gaps in pillar-based phononic crystal strips', *J. Appl. Phys.*, 2015, **118**, pp. 1–7, doi.org/10.1063/1.4936836
- Kundu, T., Banerjee, S., and Jata, K.V.: 'An experimental investigation of guided wave propagation in corrugated plates showing stop bands and pass bands', *J. Acoust. Soc. Am.*, 2006, **120**, (3), pp. 1217–1226, doi: 10.1121/1.2221534
- Miniaci, M., Mazzotti, M., Radziński, M., et al.: 'Experimental observation of a large low-frequency band gap in a polymer waveguide', *Front. Mater.*, 2018, **5**, pp. 1–9, doi.org/10.3389/fmats.2018.00008